DOI: 10.1002/cbdv.201900659

FULL PAPER

CHEMISTRY & BIODIVERSITY

Design, Synthesis, and Biological Evaluation of 2-(2-Bromo-3-nitrophenyl)-5-phenyl-1,3,4-oxadiazole Derivatives as Possible Anti-Breast Cancer Agents

Arjun H. Ananth,[a] Natarajan Manikandan,[b] Ravi Kumar Rajan,[b] Ramakrishnan Elancheran,[a] Kunasekaran Lakshmithendral,[a] Muthiah Ramanathan,[b] Atanu Bhattacharjee,[c] and Senthamaraikannan Kabilan*[a]

[a] Drug Discovery Lab, Department of Chemistry, Annamalai University, Chidambaram 608002, Tamil Nadu, India, e-mail: profdrskabilan@gmail.com

[b] Department of Pharmacology, PSG College of Pharmacy, Coimbatore 641004, Tamil Nadu, India

[c] Computational Biology Laboratory, Department of Biotechnology and Bioinformatics, North-Eastern Hill University, Shillong 793022, India

Breast Cancer (BCa) is the most often diagnosed cancer among women who were in the late 1940's. Breast cancer growth is largely dependent on the expression of estrogen and progesterone receptor. Breast cancer cells may have one, both, or none of these receptors. The treatment for breast cancer may involve surgery, hormonal therapy (Tamoxifen, an aromatase inhibitor, etc.) and oral chemotherapeutic drugs. The molecular docking technique reported the findings on the potential binding modes of the 2-(2-bromo-3-nitrophenyl)-5-phenyl-1,3,4-oxadiazole derivatives with the estrogen receptor (PDB ID: 3ERT). The 1,3,4-oxadiazole derivatives **4a**–**4j** have been synthesized and described by spectroscopic method. 2-(2-Bromo-6-nitrophenyl)-5-(4-bromophenyl)-1,3,4-oxadiazole (**4c**) was reconfirmed by single-crystal XRD. All the compounds have been tested in combination with generic Imatinib pharmaceutical drug against breast cancer cell lines isolated from Caucasian woman MCF-7, MDA-MB-453 and MCF-10A non-cancer cell lines. The compounds with the methoxy (in **4c**) and methyl (in **4j**) substitution were shown to have significant cytotoxicity, with **4c** showing dose-dependent activation and decreased cell viability. The mechanism of action was reported by induced apoptosis and tested by a DNA enzyme inhibitor experiment (ELISA) for Methyl Transferase. Molecular dynamics simulations were made for hit molecule **4c** to study the stability and interaction of the protein–ligand complex. The toxicity properties of ADME were calculated for all the compounds. All these results provide essential information for further clinical trials.

Keywords: 1,3,4-oxadiazole, breast cancer, estrogen receptor, single-crystal XRD, molecular dynamics, ADMET, cytotoxicity.

Introduction

Cancer is a class of diseases that contributes to abnormal cell growth and spread. If the ranges of the abnormal cells are not controlled, it can result in death. The second-largest source of cancer death in women worldwide, after lung cancer, is breast cancer (BCa). The risk of breast cancer deaths in a person is roughly 1 out of 38 in recent years, approximately 2.6%. It is reported from the American Cancer Society that in 2019, around 268,600 people were diagnosed and 41,760 deaths from Breast cancer were recorded.[1] Studies showed that there is a 3.1% rise in the global incidence of breast cancer every year. The ERα (estrogen receptor alpha) is essential for mammary gland development and plays a vital role in breast cancer growth. It was reported that ERα could mediate

Supporting information for this article is available on the WWW under https://doi.org/10.1002/cbdv.201900659

estrogen-induced cell proliferation in an autocrine way in ERα positive breast cancer cell lines.[2] Estrogen receptor-positive (estrogen receptor and progesterone receptor-positive) cancer patients are often first diagnosed with hormone therapy (Tamoxifen or an antagonist of aromatases).[3,4] These drugs can be given in combination with a targeted drug such as Abemaciclib (Verzenio), Ribociclib (Kisqali), Palbociclib (Ibrance) and Everolimus (Afinitor). If the cancer is not extensively responding to hormone therapy, then chemotherapy is also a treatment for women with hormone receptor-negative (ER-negative and PR-negative) cancers, since hormone therapy is not helpful in III and IV stages of diseases.[5] In contrast, chemotherapy is attributed to its effectiveness in destroying cancer cells, but the prognosis is low and affects healthy human cells as well. There are many different drugs to combat these, and formulations can be used to manage breast cancer.[6,7] The antiestrogen is used to block the effects of estrogen on cancer cells and some of the antiestrogens were developed as the drugs, Tamoxifen, Ormeloxifene, Clomifene, Bazedoxifene, Lasofoxifene, Toremifene, Nafoxifene, Raloxifene, Cyclofenil, have been used to block the estrogen signal.[8,9]

The functional modification of the 1,3,4-oxadiazole scaffold and basic interactions were observed, such as Oxolamine (antitussive), Nesapidil (antihypertensive), Furamizole (antibiotic) and Zibotentan (anticancer) and designed molecule **4c** are shown in *Figure 1*. Structural changes and the basic interactions identified from the 1,3,4-oxadiazole scaffold, such as Sulfisoxazole (antibacterial), Oxacillin (antibiotic), Linezolid (antibacterial), Toloxatone (antidepressant), Furazolidone (antibacterial), Raltegravir (anti-HIV) as shown in *Figure 2*. Oxadiazole compounds as the bioisostere of benzimidazoles and thiazoles,[10] imidazoles,[11] tetrazoles,[12] and triazoles[13,14,15] have attracted increasing attention. Recently, numerous researches have been devoting to oxadiazole compounds as a medicinal agent with an intent to discover novel chemical scaffold compounds with low toxicity, high bioactive and excellent pharmacokinetic property.[16,17] Thus, oxadiazoles are the important moieties that show more effective inhibition against various cancer cell lines such as breast cancer (MCF-7, MDA-MB231), skin cancer (HaCaT), cervical cancer (HeLa), liver cancer (HepG2), colorectal cancer (SW1116), human lung cancer cells (L2987, A549) and stomach cancer (BGC823).[18,19] In this aspect, there is a rise in the need to build novel anti-estrogen agents to combat estrogen receptor–ligand binding domain. Co-crystalized ligand-receptor interfaces can be widely used in synthetic drug design and provide a promising outlook for the discovery of an active inhibitor of breast cancer and its physicochemical properties.

The structure-based docking approach was followed for analyzing structure–activity relationships

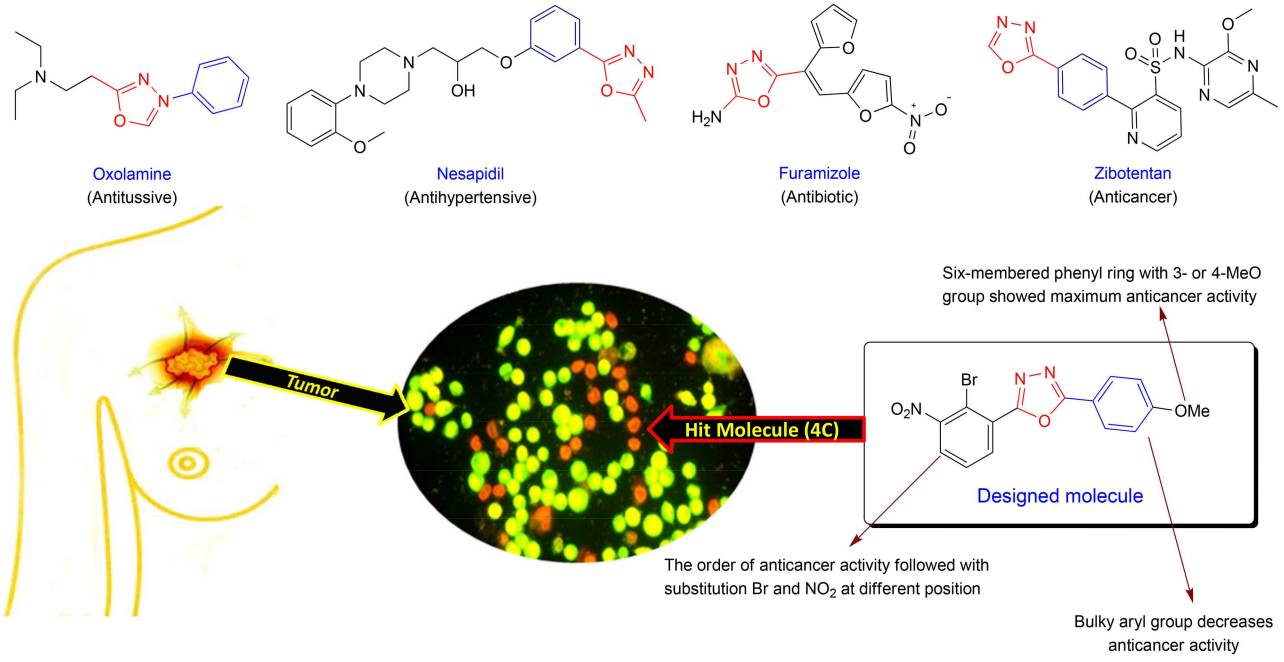

Figure 1. Therapeutic estrogen receptor targets for treating breast cancer.

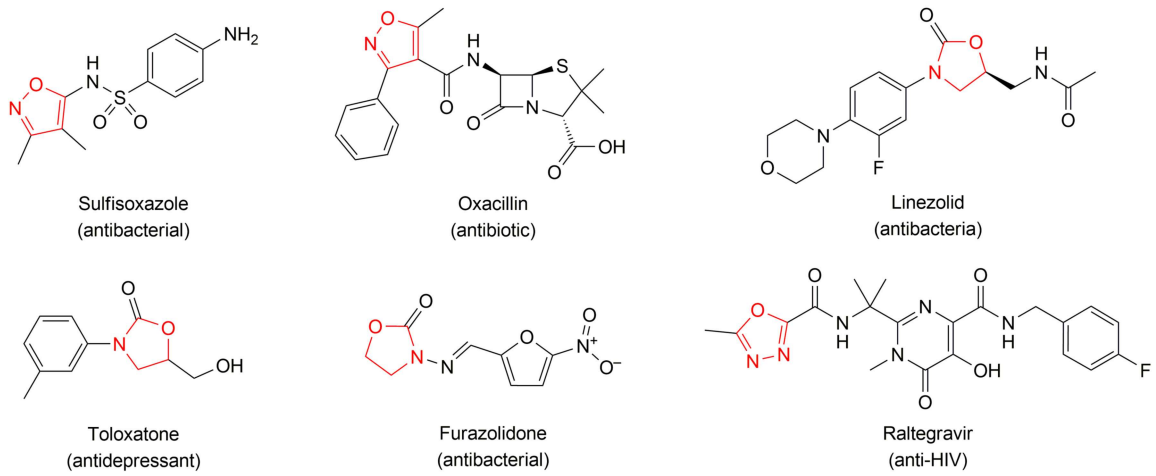

Figure 2. Some clinical oxadiazole drugs.

(SAR) of molecules for finding potentially active compounds,[20] which can be summed up. In this article, the design and development of 1,3,4-oxadiazole derivatives have been described as a novel antiestrogen. The two combined substructures 2-bromo-3-nitrobenzohydrazide ring with 1,3,4-oxadiazole scaffolds and R-carboxylic acid ring attached on the other side might show synergistic cytotoxic affects.[21] All of these findings motivated us to introduce these two moieties and to illustrate 1,3,4-oxadiazole compounds as promising anti-breast cancer agents. Compounds **4a**–**4j** were synthesized and structurally elucidated using various spectroscopic techniques (NMR, IR, and LC/MS). Additionally, the molecule **4i** has been reconfirmed by the single-crystal XRD. Compounds **4a**–**4j** have been tested against MCF-7 and MDA-MB-453 cell lines on in vitro cancer activities.[22]

Results and Discussion

In Silico Molecular Docking Studies

A structure-based virtual screening was performed using 1,3,4-oxadiazole derivatives.[23] Crystal coordinates of the inhibitor bound human estrogen receptor alpha was taken from the Protein Data Bank (PDB ID: 3ERT) and modified, the raw structure being used for the analysis.[24] The interaction between the compounds **4a**–**4j** and ERα receptors are shown in *Figure S1*. Molecular docking study suggests that hydrophobic interactions with amino acid residues Arg394, Glu353, Asp351, Thr347, and Leu346 contributed to binding affinity. Further, molecule **4c** had an H-bond interaction with Arg394 and a lone water molecule (2.04 Å). It is apparent from the compound **4c**–ERα complex that the active site of ERα is composed of a largely hydrophobic pocket; consequently, the selective binding of possible anti-breast cancer agents should rely primarily on these hydrophobic and H-bond interactions.

Van der Waals interactions with the surrounding hydrophobic residues are found with compounds **4a**–**4j**, such as Phe404, Ala350, Leu349, Leu346, Met343, Met528, Leu525, Trp383, Leu384, Leu387, Met308, Leu428, Leu391. Hydrogen bonds through the methoxy group with H_2O residues are found in compound **4c** and also forms two salt bridge through a nitro group with residues Arg394 and Glu353 in the helix 12 in compounds **4c**, **4d**, and **4g**. The ligand interaction diagram of compound **4c** and the standard Imatinib with estrogen receptor α have been demonstrated in *Figure 3*. Among the synthesized compound, molecule **4c** have shown the highest docking score (−7.84 kcal/mol) and glide energy score (−7.84 kcal/mol). Respective Docking score and glide energy score with interacting amino acid residues of synthesized compounds **4a**–**4j** are shown in *Table 1*. Imatinib and Tamoxifen (standard drugs) showed a glide score of −9.178 and −12.541 kcal/mol, respectively, and binding energy, −55.298 and −56.295 kcal/mol, respectively. These results are well conventional and were reported.

Chemistry

A molecular hybridization approach was followed for 2-(2-bromo-3-nitrophenyl)-5-phenyl-1,3,4-oxadiazole

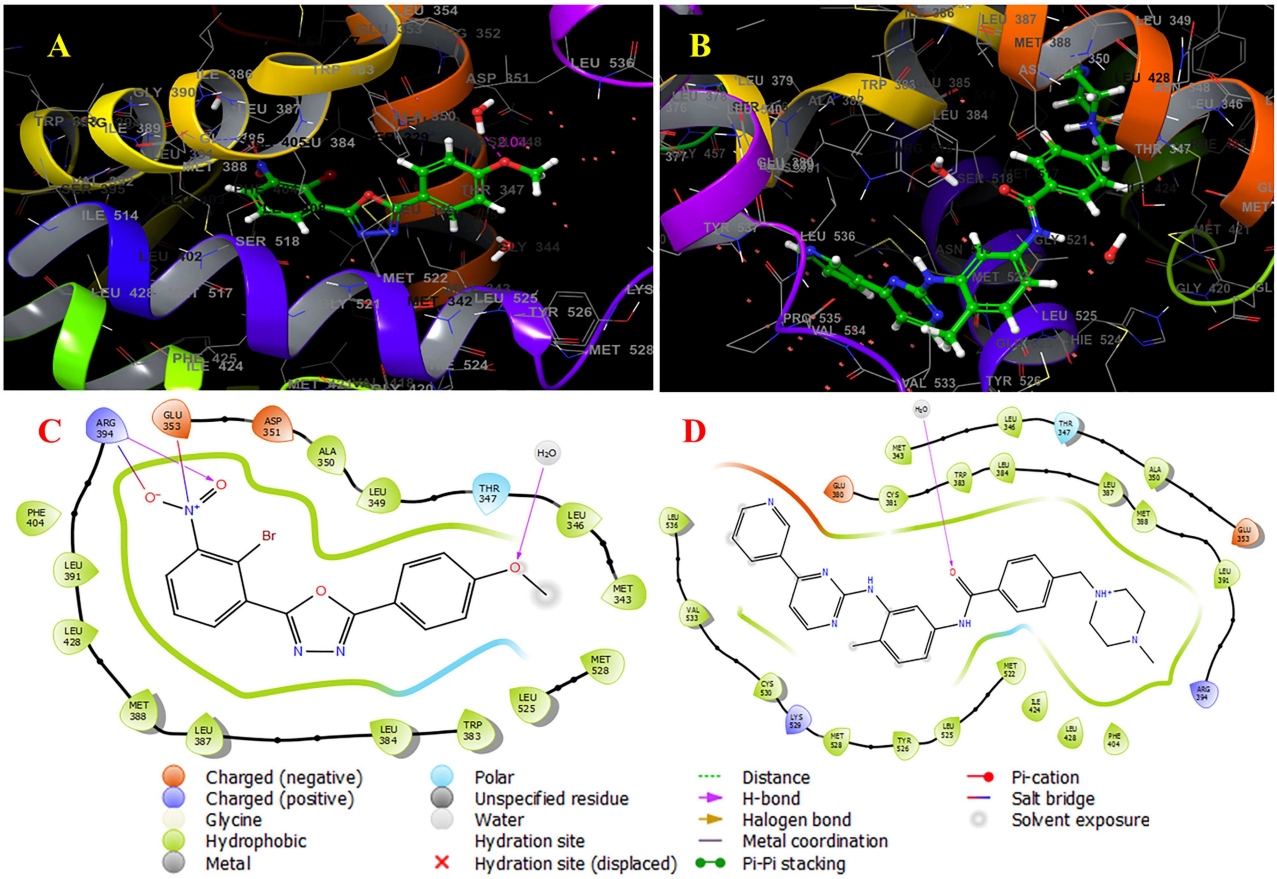

Figure 3. Predicted binding mode of compound **4c** (*Figure 3A* and *3 C*) and standard Imatinib (*Figure 3B* and *3D*) with protein PDB: 3ERT.

Table 1. Docking score, binding energy and compound mode expected (**4a**–**4j**).[a]

Compound	Glide gscore	Glide evdw	Glide ecoul	Glide energy	Interacting residues
4a	−7.767	−37.401	1.269	−36.133	–
4b	−7.277	−40.795	−0.963	−41.758	ARG394, GLU353, H_2O
4c	−7.842	−40.592	−2.208	−42.8	ARG394, GLU353, H_2O
4d	−6.955	−40.857	−0.903	−41.76	ARG394, GLU353
4e	−6.992	−39.71	1.242	−38.468	–
4f	−6.366	−37.391	0.133	−37.258	–
4g	−7.277	−40.795	−0.963	−41.758	ARG394, GLU353, H_2O
4h	−7.237	−45.628	−0.13	−45.758	–
4i	−7.171	−39.166	−0.277	−39.443	–
4j	−7.612	−38.321	0.677	−37.644	–
Imatinib	−9.178	−51.793	−3.505	−55.298	–
Tamoxifen	−12.541	−49.629	−6.666	−56.295	H-Bond interaction with H_2O

[a] Glide evdw = Van der Waals interaction energies, glide ecoul = Coulomb interaction energies

derivatives. The synthetic route for the compounds was designed by keeping 1,3,4-oxadiazole scaffold as a targeting estrogen receptor alpha for the treatment of breast cancer. Carboxylic acid was first transformed to its corresponding ester by an esterification process, followed by refluxing with hydrazine hydrate in ethanol at 100 °C for 6 h; this culminated in the synthesis of carbohydrazides **3a** and **3b**. Additionally,

the compounds **4a**–**4j** were achieved by the reaction of compounds **3a** and **3b** with benzoic acid and phosphoryl chloride refluxing at 100 °C in the presence of ethanol for 8 h (*Scheme 1*). Column chromatography was used to purify all the compounds, and spectroscopic techniques confirmed their structures.[25] The yields and melting points of the compounds were recorded and shown in the *Experimental Section.*

The compound **4i** was recrystallized in DMSO/chloroform by slow evaporation at room temperature.[26] The crystal of **4i** belongs to the monoclinic system with space group belonging to $P2_1/c$, a = 15.952(4) Å, b = 6.9526(19) Å, c = 14.826(4) Å, $\alpha = 90°$, $\beta = 116.704(13)°$, $\gamma = 90°$, Z = 4.[27,28] The ORTEP diagram of the compound **4i** was illustrated in *Figure 4*. The unit cell diagram of the compounds **4i** is revealed in *Figure S2*. Description of the refining of the crystal structure and parameters are described in *Table S1*. Liquid chromatography was used to determine the purity of the compounds **4a**–**4j**. Compound **4a**–**4j** had the purity of 98% and above as shown in liquid chromatogram spectra. All spectroscopic analysis confirmed the structures of the compounds **4a**–**4j** as shown in *Table S2*, and the purity of all the compounds is shown in LC spectra.

Biological Evaluation

Compounds **4a**–**4j** were tested for cytotoxic activity against breast cancer cell lines MCF-7 and MDA-MB-453, and non-cancerous cell lines MCF-10 A.[29] Cell viability assay (MTT assay) showed that compounds **4a**–**4j** had more significant inhibition on cancerous cells and were non-toxic to non-cancerous cells (IC_{50} >

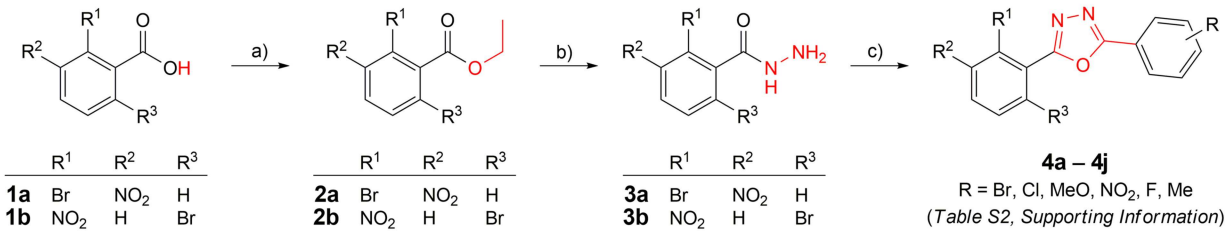

a) Conc. H_2SO_4 in 20 ml EtOH, reflux at 100 °C for 16 h. b) Hydrazine hydrate in 10 ml EtOH, reflux at 100 °C for 1 h.
c) R–COOH, $POCl_3$, reflux 100 °C for 1 h.

Scheme 1. Synthesis of 1,3,4-oxadiazole derivatives.

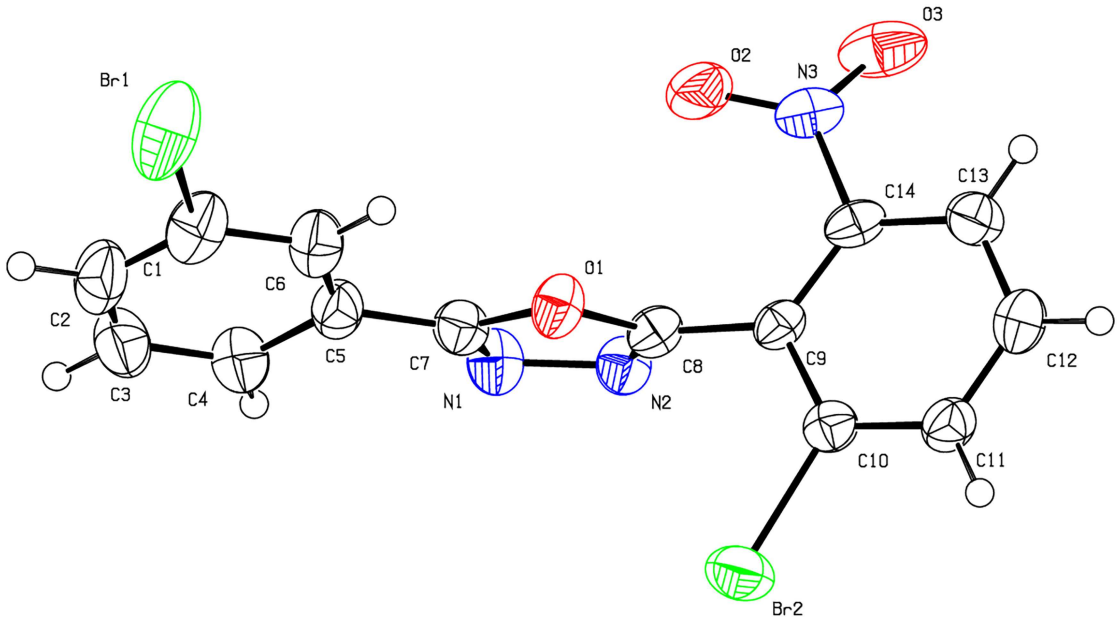

Figure 4. ORTEP structure of compound **4i**.

100 μM). The IC_{50} values of the compounds **4a**–**4j** were ranged from 12.16 to 48.43 μM. These findings indicated that compounds **4a**–**4j** have significant cytotoxic potential towards MCF-7 and MDA-MB-453 cell lines. The IC_{50} values of the standard drug Imatinib towards MCF-7 and MDA-MB-453 was observed as 6.31 μM and 12.78 μM, respectively. Among all, the molecule **4c** showed an equipotent inhibition (IC_{50} = 12.50 μM) of the MDA-MB-453 cell lines as compared to standard Imatinib. The IC_{50} values of all test compounds in different cell lines are shown in *Table 2*. Cell viability of molecule **4c** against MCF-7 is shown in *Table 3*. Cell viability of MCF-7 cells against molecule **4c** is demonstrated in *Figure 5*. Selectivity index calculation showed that Imatinib was more selective (SI > 16) for MCF-7 followed by molecules **4c** (SI > 8) and **4j** (SI > 7). On the other hand, molecule **4c** and Imatinib showed similar selectivity (SI > 8) for MDA-MB-453 followed by molecule **4j** as shown in *Table 4*. This data suggest that **4c** and **4j** have greater potential as anticancer agents, especially molecule **4c** against MCF-7 and were non-toxic to MCF-10A cell lines.

Our study suggests that when the methoxy group was introduced to the phenyl ring, the inhibitory activity was improved for the derivatives of 1,3,4-oxadiazole. R-group substitution with a methoxy group has already shown to have anticancer activity.[30] When the methyl group is substituted with other groups, the anticancer activity was found to be lower. Similarly, the R-group substitution of bromine was found to be better than fluorine. The toxicity

Table 2. Analysis of molecules **4a**–**4j** and standard drug for cytotoxic studies.

Ligand	MCF-7 [μM]*[a]	MDA-MB-453 [μM][a]	MCF-10 A [μM][a]
4a	34.52 ± 2.8	48.19 ± 2.1	68.17 ± 2.03
4b	48.43 ± 1.82	> 50	> 100
4c	**12.16 ± 1.43**	**12.50 ± 1.14**	**> 100**
4d	44.23 ± 2.1	> 50	> 100
4e	> 50	> 50	> 100
4f	27.3 ± 0.57	42.26 ± 1.52	82.17 ± 2.73
4g	> 50	> 50	> 100
4h	21.68 ± 4.84	39.41 ± 2.98	78.17 ± 2.13
4i	37.57 ± 2.39	47.27 ± 1.69	> 100
4j	14.16 ± 0.64	28.20 ± 2.87	> 100
Imatinib[b]	6.31 ± 1.4	12.78 ± 2.1	> 100

[a] The values are the mean ± standard deviation (SD) of three independent experiments performed in triplicate. [b] Positive control. * IC_{50} of the compounds stimulated by 1 nM DHT.

Table 3. Dose-response of **4c** in Cytotoxicity assay

Concentration [μM]	% Inhibition	% Cell viability
Control	0.01	99.99
1	12.5	87.5
3	24.6	75.4
10	40.2	59.8
100	90.6	9.4

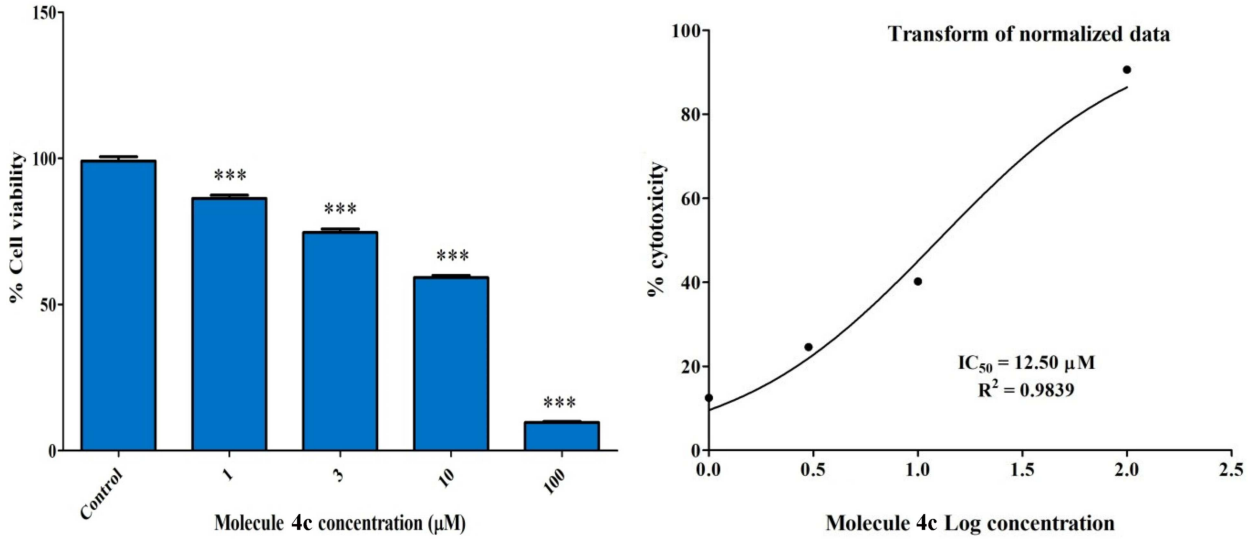

Figure 5. MTT assay. The bar graph shows the dose dependent decrease in cell viability when cells were treated with compound **4c**. The line graph on the right depicts the dose dependent increase in cytotoxicity, and the IC_{50} of the compound **4c** was found to be 12.50 μM. Experiments were done in triplicates. Values are expressed as mean ± SD. Data were analyzed by one-way ANOVA followed by Tukey's post hoc test. ***$P < 0.001$, as compared to the control group.

Table 4. Selectivity index of test molecules was calculated relative to MCF-10A (non-cancerous cell lines).

Molecules	MCF-7	MDA-MB-453
4a	2	1
4b	>2	>2
4c	>8	>8
4d	>2	>2
4e	>2	>2
4f	3	2
4g	>2	>2
4h	4	2
4i	>3	>2
4j	>7	>4
Imatinib	>16	>8

profile of compounds **4c** and **4j** was also tested against the MCF-10A cell lines (normal mammary cell) and no toxicity was observed. The compounds **4c** and **4j** have potential anti-breast cancer activity. It was also observed that the methoxy, methyl, and bromo groups have greatly influenced anticancer activity.

AO/EtBr staining was performed to visualize the apoptosis in tested compound treated cells. The stained image showed that the synthetic compound **4c** treated, had a higher number of apoptotic cells indicated by the yellow color in MCF-7 cell lines. The first step of cell disassembly detected during treatment was cell membrane blebbing (light green or yellow). Live cells have normal nuclei that have ordered structures and green chromatin. The fluorescence images of AO/EtBr staining are demonstrated in *Figure 6*.

When DNA methylation takes place in the promoter region of the gene, it results in silencing of genes, such as tumor-suppressing genes. In a cancer cell, hyper methylation occurs which results in malformation of tumor suppressor function. DNA methylation takes place at the 5th position of the cytosine ring, where methyl group is added covalently. The projection of these methyl groups in the DNA grooves interferes with the transcription of tumor suppressor genes.[31] DNA methyltransferases (DNMTs) are the enzymes which catalyze the addition of methyl group to the cytosine. DNMTs such as DNMT1, DNMT3a and DNMT3b are mammalian specific. DNMT1 assay suggested that compound **4c** had potential DNMT1 inhibitory activity at both lower and higher dose. The percentage of DNMT1 enzyme inhibition is shown in *Table 5*. The present experimental data suggested that compound **4c** can also be tested in the diagnosis of breast cancer with DNMT isoform. A concentration gradient response was found in the enzyme inhibition

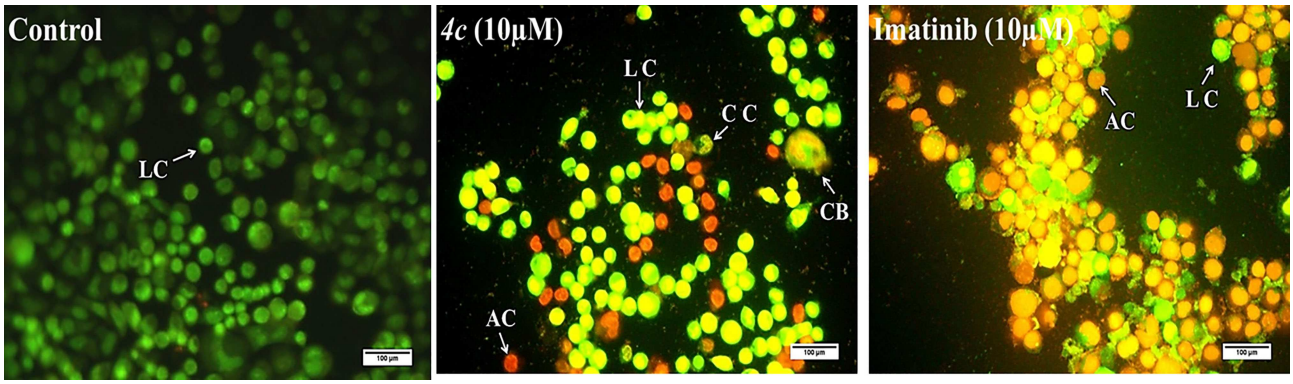

Figure 6. Acridine orange/ethidium bromide fluorescent staining. The changes in morphology of breast cancer cells treated with 10 µM of compound **4c** and Imatinib. LC, AC, CB and CC indicate the live cells, apoptotic cells, cell membrane blebbing and chromatin condensation, respectively. The image is visualized using 20X resolution in an inverted microscope. Bar 100 µm.

Table 5. DNMT inhibition assay.

DNMT 1 Inhibition assay Test compound	1 µM OD ± SD	% Inhibition	100 µM OD ± SD	% Inhibition
Control	1.519 ± 0.062			
5AZA	1.302 ± 0.072	11.9	0.892 ± 0.086	38.9
4c	1.322 ± 0.790	12.95	1.097 ± 0.652	24.3

experiment, and the high concentration showed 24.3 % of inhibition.

ADME

In the asses of drug-like properties and pharmacokinetic properties, ADME (adsorption, delivery, metabolism, and elimination) has an essential role. Due to poor ADME properties, there are several drugs which failed during clinical trials, so it is crucial during drug discovery. ADME characteristics of compounds **4a**–**4j** are shown in *Table S3*. All tested compounds were found to comply with the Lipinski rule of five and the rule of three. This suggests that all molecules have drug-like characteristics. The oral bioavailability of test compounds **4a**–**4j** was also found to be better. Prediction for IC_{50} of molecules **4a**–**4j** for HERG K+ blockage was also found to be acceptable.[32]

Table 6. Description study of simulation performance after equilibrium.

S. No.	Properties	Statistical parameters
1	Simulation period [ns]	50.098
2	Degrees of freedom	35123
3	Number of atoms	31259
4	Average total energy [kcal/mol]	45199.046
5	Average potential energy [kcal/mol]	55518.371
6	Temperature [K]	300
7	Pressure [bar]	14.244
8	Volume [$Å^3$]	56247.958

Molecular Dynamics Simulations

During molecular dynamics study, simulation trajectory was fixed for 50 ns.[33] All the physical parameters used during the simulation are summarized in *Table 6*. The RMSD (root-mean-square deviation) of the ERα–**4c** complex is shown in *Figure 7*, and it was found to be fixed below 3 Å. The root mean square deviation of the **4c**–3ERT system achieved a stable structure. The RMSD protein began at 1.6 Å and then stabilized in 2.8 Å for ligand. However, RMSD started with 1.8 Å and stabilized with 2.0 Å. For small globular proteins, RMSD fluctuation of the 1–3 Å scale is perfectly acceptable. Changes greater than 3 Å indicated greater conformational changes, which are not preferable. The nitrogen atom of 1,3,4-oxadiazole scaffold displayed hydrogen bond interaction with THR347 (47 %), ARG394 (10 %), and ASP351 bridged with H_2O (7 %), respectively. Also, the π–π stacking relationship has been found in the binding pocket of 3ERT with HIS524

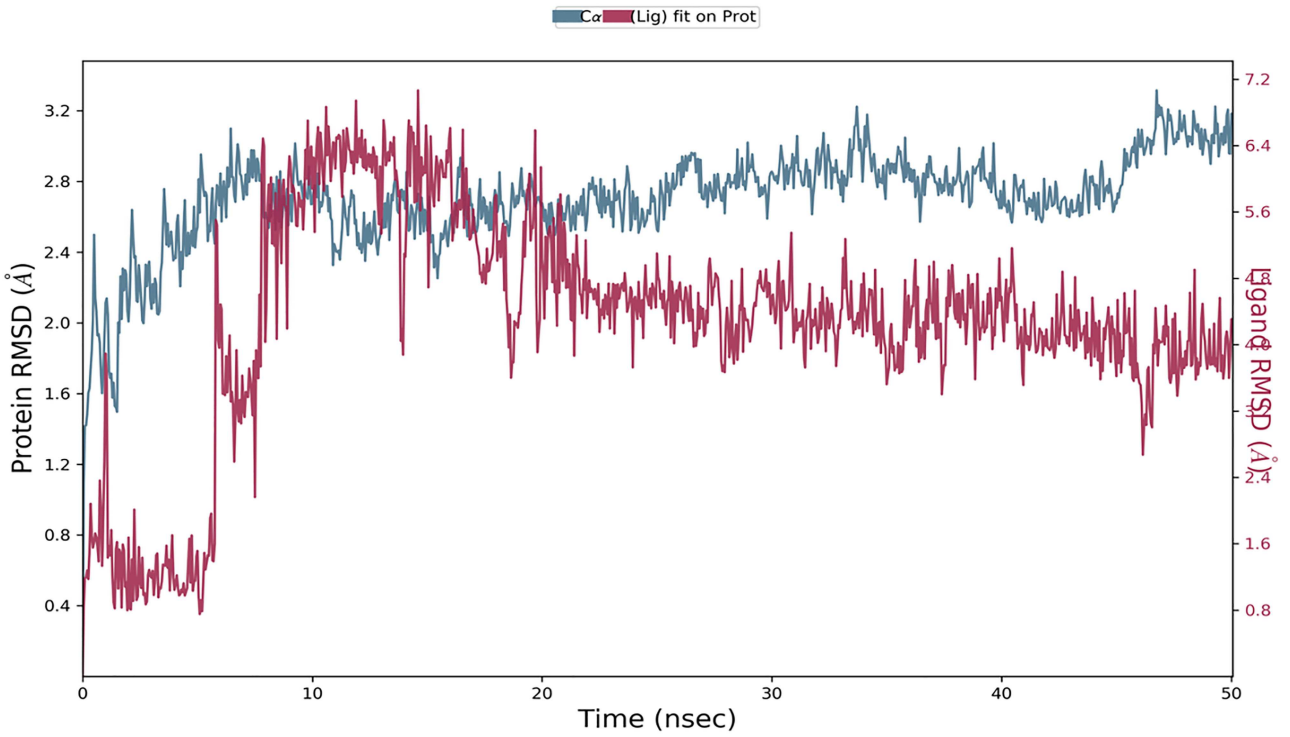

Figure 7. The compounds of **4c** and 3ERT complex for RMSD were obtained.

(14%) and PHE404 (8%). *Figure 8* demonstrates the interaction fraction of amino acid and compound **4c** and the percentage interaction that amino acid residue made with the compound **4c**.

Conclusions

In the current study, the molecular docking strategy for the estrogen receptor was used to design a series of molecules. The ligand's binding affinities and the exact interaction simulations of molecular dynamics confirm the molecular docking analysis. The compounds **4a**–**4j** were successfully synthesized, and the activity against breast cancer was illustrated. The compound **4i** was reconfirmed through single-crystal XRD analysis. Compounds **4c** and **4j** were shown to be the most reliable of the series especially against MCF-7 with IC_{50} of 12.16 ± 1.43 and 14.16 ± 0.64 μM, respectively. For the MDA-MB-453 cell lines, the toxicity was also tested for compounds **4a**–**4j**. The highest glide score −7.84 kcal/mol and glide energy −42.8 kcal/mol with the estrogen receptor, respectively, indicated the binding efficiency of compound **4c**. Further, the results show that the compounds with methoxy and methyl substitutions at R have more significant interactions and anticancer activity than others. In contrast, the DNMT inhibition and mediated apoptosis are significantly inhibited by the compound **4c**. We intend to analyze the target site and research the behavior of these active compounds in vivo model.

Experimental Section

In Silico Molecular Docking

The X-ray crystal coordinates of the estrogen receptor were taken from the archive of the RCSB protein data bank (PDB ID: 3ERT, Resolution: 1.9 Å). The protein structure was refined, and energy was minimized (OPLS-2005) using Prep Wiz module of Maestro 11.1. The grid was generated using the Grid generator docking wizard. The 2D-structures of molecules were structured computationally using chem draw ultra 12.0. These molecules were then converted to its energy minimized 3D structure using LigPrep module of Maestro 11.1. GLIDE module of Maestro 11.1 was used for molecular docking study. All molecules were docked within the grid-generated receptor of estrogen receptor. Post-docking minimization was also performed to improve the geometry of the generated poses. After post-docking minimization, top poses were selected based on docking score/e-model.[34]

Chemistry

All the reagents and solvents are of analytical reagent grade purchased from retail suppliers such as Spectrochem, Alfa Aesar, Sigma–Aldrich, etc. Reactions were tracked using a separate solvent method with various polarities using thin-layer chromatography (TLC; Merck silica gel 60 F_{254}), and spots were visualized in the UV light. The open capillary system was used in the Raagaa melting point device to record melting points. The Thermo Scientific FT-IR spectrophotometer instrument was used to record IR spectra using KBr for preparing pellets. In FT-IR frequencies, the compounds exhibited the absorption bands at

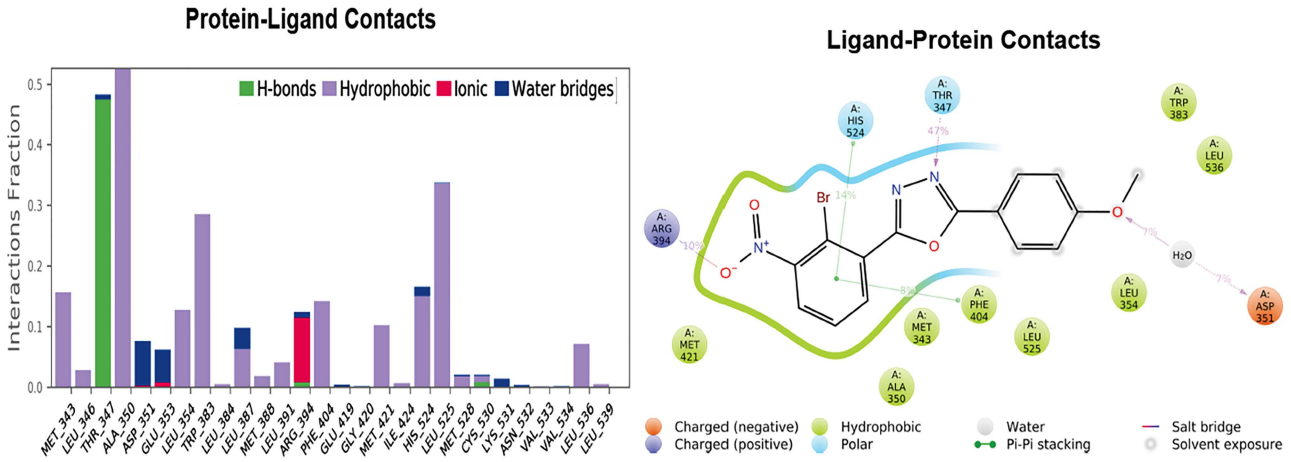

Figure 8. The histogram and the interactions of compound **4c** with protein 3ERT in molecular dynamic simulation.

650 cm^{-1} due to C–Br, at 1220–1330 cm^{-1} due to C–C stretching, C–Cl stretching at 725 cm^{-1}, methyl group at 2917 cm^{-1}, methoxy group at 2845.24 cm^{-1}, C–O stretching at 1020 cm^{-1}, C=C stretching at 1650 cm^{-1} and 1605–1590 cm^{-1} due to imine (C=N) stretching, confirming the structures of compounds **4a**–**4j**. Using (D_6)DMSO solvent at room temperature, the ^{1}H- and ^{13}C-NMR spectra are registered at 400 MHz using Bruker AVANCE III. The compounds revealed in ^{1}H-NMR spectra that aromatic proton signals at 7.5–9.0 ppm and aliphatic protons signal at 2.0–4.0 ppm. Signal detected at 120–150 ppm in ^{13}C-NMR range attributable to aromatic and CH=N signals at 20–30 ppm at aliphatic carbon signals. Mass spectra of compounds were recorded on an Agilent LC/MS Spectrometer. There were significant parent ion peaks in the compounds. The percentages of purity of the molecules **4a**–**4j** are shown in the *Supporting Information*, which was characterized by liquid chromatography.

Step I. General Protocol for Ester Synthesis

A mixture of carboxylic acid (0.01 mol), ethanol (20 ml), and a catalytic amount of concentrated sulfuric acid was taken in a round bottom flask and refluxed for 12 h. The excess of ethanol was distilled off. The product was transferred to a separating funnel, holding roughly 250 ml of distilled water after cooling. The synthesized ester was repeatedly extracted with 50 ml chloroform. The organic layer was treated with distilled water and dried with sodium sulfate. Chloroform was distilled off under condensed pressure to give the ester, which was weighed after drying.

Step II. Preparation of Carbohydrazide

A mixture of ester (0.01 mol), hydrazine hydrate (0.015 mol), and 10 ml of ethanol was taken in a round bottom flask and refluxed for 6 h at 100 °C. Under higher pressure, ethanol and excess hydrazine hydrate were distilled off. Further, the precipitate was filtered and recrystallized with ethanol.

Step III. Standard Method for the Preparation of Compounds **4a**–**4j**

A mixture of carbohydrazide (0.01 mol), benzoic acid (0.01 mol), and phosphoryl chloride ($POCl_3$) was refluxed for 8 h at 100 °C, then cooled and ice cubes were poured and neutralized by potassium carbonate. The solid precipitate was filtered, washed with water, and then extracted using ethyl acetate and then purified by column chromatography with hexane as eluent.

Experimental Evidence

The synthesized compounds **4a**–**4j** are described by IR, NMR, and LC/MS, and all the data match with the structures suggested herein.

2-(2-Bromo-3-nitrophenyl)-5-(3-bromophenyl)-1,3,4-oxadiazole (**4a**). Yield: 84%. M.p. 165–167 °C. Brown solid. ^{1}H-NMR ((D_6)DMSO, 400 MHz): 8.49 (d, J = 8.4, 1H, Ar–H), 8.43 (d, J = 7.6, 1H, Ar–H), 8.29 (s, 1H, Ar–H), 8.17 (d, J = 7.6, 1H, Ar–H), 8.04–7.97 (m, 2H, Ar–H), 7.68 (t, J = 8, 1H, Ar–H). ^{13}C-NMR ((D_6)DMSO, 100 MHz): 164.35, 160.34, 149.79, 139.27, 135.98, 135.49, 132.46, 129.54, 126.34, 125.99, 125.36, 124.96, 123.17, 120.57. MS: calc. for $C_{14}H_7Br_2N_3O_3$ $[M+H]^+$: 422.8854; found: 423.9010.

2-(2-Bromo-3-nitrophenyl)-5-(4-chlorophenyl)-1,3,4-oxadiazole (**4b**). Yield: 90%. M.p. 162–164 °C. Light brown solid. ^{1}H-NMR ((D_6)DMSO, 400 MHz): 8.33 (d, J = 7.2, 1H, Ar–H), 8.42 (d, J = 8, 1H, Ar–H), 8.14 (d, J = 8, 2H, Ar–H), 7.897–7.858 (m, 1H, Ar–H), 7.73 (d, J = 8, 2H, Ar–H). ^{13}C-NMR ((D_6)DMSO, 100 MHz): 164.49, 162.49, 152.77, 137.73, 135.02, 131.61, 130.30, 130.22, 130.08, 129.18, 127.78, 127.48, 122.28, 112.92. MS: calc. for $C_{14}H_7BrClN_3O_3$ $[M+H]^+$: 378.9359; found: 379.9435.

2-(2-Bromo-3-nitrophenyl)-5-(4-methoxyphenyl)-1,3,4-oxadiazole (**4c**). Yield: 92%. M.p. 166–168 °C. Pale white solid. ^{1}H-NMR ((D_6)DMSO, 400 MHz): 3.87 (s, 1H, OCH_3), 8.311 (d, J = 1.6, 1H, Ar–H), 8.29–8.21 (m, 1H, Ar–H), 8.06 (d, J = 8.8, 2H, Ar–H), 7.87 (t, J = 8, 1H, Ar–H), 7.19 (d, J = 8.8, 2H, Ar–H). ^{13}C-NMR ((D_6)DMSO, 100 MHz): 165.19, 162.89, 161.86, 152.74, 134.91, 130.40, 130.26, 129.26, 128.88, 127.73, 127.59, 115.63, 115.48, 115.31, 112.84, 56.06. MS: calc. for $C_{15}H_{10}BrN_3O_4$ $[M+H]^+$: 374.9855; found: 375.9431.

2-(2-Bromo-3-nitrophenyl)-5-(4-bromophenyl)-1,3,4-oxadiazole (**4d**). Yield: 86%. M.p. 175–178 °C. Pale white solid. ^{1}H-NMR ((D_6)DMSO, 400 MHz): 8.34 (d, J = 1.2, 1H, Ar–H), 8.32 (d, J = 1.6, 1H, Ar–H) 8.26–7.90 (m, 2H, Ar–H), 7.88–7.84 (m, 3H, Ar–H). ^{13}C-NMR ((D_6) DMSO, 100 MHz): 164.61, 162.51, 152.78, 135.03, 133.14, 133.01, 130.31, 129.28, 127.79, 126.66, 122.63,

112.92. MS: calc. for $C_{14}H_7Br_2N_3O_3$ $[M+H]^+$: 422.8854; found: 423.8830.

2-(2-Bromo-3-nitrophenyl)-5-(3-nitrophenyl)-1,3,4-oxadiazole (**4e**). Yield: 83%. M.p. 178–180 °C. White solid. ^{1}H-NMR ((D$_6$)DMSO, 400 MHz): 8.81 (s, 1H, Ar–H), 8.52–8.51 (m, 2H, Ar–H), 8.39 (d, J=7.6, 1H, Ar–H), 8.26 (d, J=7.242, 1H, Ar–H), 7.99–7.88 (m, 2H, Ar–H). ^{13}C-NMR ((D$_6$)DMSO, 100 MHz): 163.73, 162.86, 152.82, 148.81, 144.89, 13515, 133.46, 131.98, 130.36, 127.90, 127.31, 124.93, 121.87, 113.00. MS: calc. for $C_{14}H_7BrN_4O_5$ $[M+H]^+$: 389.9600; found: 390.8805.

2-(2-Bromo-3-nitrophenyl)-5-(6-fluoro-2*H*-1-benzopyran-2-yl)-1,3,4-oxadiazole (**4f**). Yield: 88%. M.p. 168–170 °C. Pale white solid. ^{1}H-NMR ((D$_6$)DMSO, 400 MHz): 8.29–8.23 (m, 1H, Ar–H), 7.90–7.861 (m, 1H, Ar–H), 7.522–7.495 (m, 1H, Ar–H), 7.194–7.65 (m, 5H, Ar–H). ^{13}C-NMR ((D$_6$)DMSO, 100 MHz): 161.71, 161.64, 156.96, 147.51, 146.78, 144.89, 141.43, 139.66, 136.32, 135.06, 130.28, 127.84, 127.72, 126.42, 123.53, 113.16, 105.52. MS: calc. for $C_{17}H_9BrFN_3O_4$ $[M+H]^+$: 416.9760; found: 417.5197.

2-(2-Bromo-3-nitrophenyl)-5-(3-chlorophenyl)-1,3,4-oxadiazole (**4g**). Yield: 86%. M.p. 190–192 °C. Pale white solid. ^{1}H-NMR ((D$_6$)DMSO, 400 MHz): 8.32–8.29 (m, 1H, Ar–H), 8.28–8.20 (m, 1H, Ar–H), 8.14–8.11 (m, 2H, Ar–H), 7.89–7.86 (m, 1H, Ar–H), 7.84–7.69 (m, 2H, Ar–H). ^{13}C-NMR ((D$_6$)DMSO, 100 MHz): 164.53, 162.49, 135.28, 135.02, 130.41, 130.31, 130.20, 129.18, 129.02, 128.10, 122.20, 112.88.MS: calc. for $C_{14}H_7BrClN_3O_3$ $[M+H]^+$: 378.9359; found: 379.6727.

2-(2-Bromo-3-nitrophenyl)-5-{1-[4-(2-methylpropyl)phenyl]ethyl}-1,3,4-oxadiazole (**4h**). Yield: 89%. M.p. 158–160 °C. Pale white solid. ^{1}H-NMR ((D$_6$)DMSO, 400 MHz): 8.44–8.40 (m, 1H, Ar–H), 8.33–8.27 (m, 2H, Ar–H), 8.19–8.17 (m, 1H, Ar–H), 8.11–8.08 (m 1H, Ar–H), 7.92–7.88 (m, 1H, Ar–H), 7.82–7.733 (m, 1H, Ar–H), 2.50 (s, 6H, 2 CH_3), 1.986 (s, 1H, CH), 1.911 (s, 1H, CH), 1.23 (s, 3H, CH_3), 0.84 (d, J=6.4, 2H, CH_2). ^{13}C-NMR ((D$_6$)DMSO, 100 MHz): 168.74, 164.99, 153.66, 142.04, 140.93, 137.55, 129.73, 129.59, 129.56, 126.97, 126.80, 121.14, 44.98, 37.11, 30.13, 22.35, 21.58, 19.65. MS: calc. for $C_{20}H_{20}BrN_3O_3$ $[M+H]^+$: 429.0688; found: 430.0988.

2-(2-Bromo-6-nitrophenyl)-5-(4-bromophenyl)-1,3,4-oxadiazole (**4i**). Yield: 84%. M.p. 168–170 °C. Brown solid. ^{1}H-NMR ((D$_6$)DMSO, 400 MHz): 8.39 (d, J=8, 1H, Ar–H), 8.32 (d, J=8, 1H, Ar–H), 8.13–7.86 (m, 2H, Ar–H), 7.84–7.60 (m, 3H, Ar–H). ^{13}C-NMR ((D$_6$) DMSO, 100 MHz): 167.26, 165.07, 160.20, 149.74, 139.22, 135.45, 133.32, 132.97, 132.18, 131.76, 129.99, 129.16, 129.11, 125.27. MS: calc. for $C_{14}H_7Br_2N_3O_3$ $[M+H]^+$: 422.8854; found: 423.9010.

2-(2-Bromo-6-nitrophenyl)-5-(4-methylphenyl)-1,3,4-oxadiazole (**4j**). Yield: 87%. M.p. 180–182 °C. Dark brown solid. ^{1}H-NMR ((D$_6$)DMSO, 400 MHz): 8.39 (d, J=8.4, 1H, Ar–H), 8.34 (d, J=8, 1H, Ar–H), 8.23–8.17 (m, 1H, Ar–H), 8.06–8.01 (m, 1H, Ar–H), 7.95–7.93 (m, 1H, Ar–H), 7.20–7.15 (m, 2H, Ar–H), 2.508 (s, 3H, CH_3). ^{13}C-NMR ((D$_6$)DMSO, 100 MHz): 164.61, 162.50, 152.77, 135.02, 133.01, 129.28, 129.14, 127.79, 127.46, 126.67, 122.93, 122.62, 112.92, 29.46. MS: calc. for $C_{15}H_{10}BrN_3O_3$ $[M+H]^+$: 358.9906; found: 360.0181.

Single-Crystal XRD

The X-ray diffraction studies were reported for the crystal of compound **4i** by Bruker axes kappa apex 2, CCD diffractometer with graphite MoK_α monochromated radiation at Annamalai University, Chidambaram, India. SHELXS-97 resolved the structure and redeveloped it using the least square complete matrix techniques. Both hydrogen atoms have been isotropically refined, and non-hydrogen atoms have been anisotropically refined.

Biological Evaluation

In Vitro Studies. During our study, all cell lines were procured from the National Center for Cell Science, Pune, India. Three types of cell lines were used during the study. MCF-7 and MDA-MB-231 cell lines were derived from the metastatic site of the mammary gland, and MCF 10 A cell lines were derived from a normal mammary gland. Culture condition for all cell lines was composed of Dulbecco's modified Eagle media, 10% fetal bovine serum (FBS; Gibco by life technologies; Product code: 12676–029) and 1% penicillin-streptomycin (Himedia; Product code: A004-5X 100 ML). Initially, cells were cultured in a T25 flask and kept under incubation (37 °C, 5% CO_2). Once the cell confluency reached 70–80%, the cells were detached from the surface using 2 ml of 0.05% trypsin. The cells were then centrifuged, and the pellet was collected and re-dispersed in 2 ml of growth media. Cells were counted using cell counter and seeded in 96-well plate at a density of 5000 cells/well. MTT assay was performed to evaluate the anticancer activity of the test drug. Cells were incubated for 48 h with

different concentrations of the test drug, i.e., 1, 3, 10 and 100 μM, in triplicate. One set of the well was incubated with DMSO (control), and one set was kept as blank (without drug and DMSO). After 48 h, media was removed, and cells were washed using phosphate buffer saline (PBS). 3-(4,5-Dimethylthiazol-2-yl)-2,5-diphenyltetrazolium bromide (MTT) was added in the media at a final concentration of 0.5 mg/ml, and the same culture media were used to incubate cells for 4 h. After 4 h, media was removed, and formosan crystals were solubilized in 50 μl/well DMSO with gentle shaking and absorbance was measured colorimetrically at 570 nm.[35,36]

Dual Fluorescent Staining Acridine Orange (AO)/Ethidium Bromide (EtBr)

Cells were seeded in a six-well plate at a density of 5×10^5 cells/well and incubated for 24 h. Cells were cultured using Dulbecco's modified Eagle media, 10% fetal bovine serum (FBS; Gibco by life technologies; Product code: 12676-029) and 1% penicillin-streptomycin (Himedia; Product code: A004-5X100ML). Once the cells were attached, and morphology was clear, cells were treated with different concentrations (1, 3, 10, 100 μM) of test drug and were kept under incubation (37 °C, 5% CO_2) for 48 h. After 48 h, the culture media were removed, and cells were washed with PBS. AO/EtBr staining was performed at a concentration of 100 μg/ml AO (100 μl) and 100 μg/ml EtBr (100 μl) and cells were visualized immediately under fluorescence microscope at λ_{exe} 460 nm and maximum λ_{emi} of 650 nm.[37,38]

Enzyme Inhibitor Assay of DNA Methyl Transferase

DNA methylation is an essential indicator of human cancer for silencing tumor-suppressing the genes and has an equivalent significance to classic genetic mutations.[39] Eight isoforms of DNA methyltransferases (DNMT) were identified, and among them, three isoforms were focused on much. DNMT 3A and DNMT 3B involved in the methylation process and DNMT are responsible for the maintenance of methylation.[40] DNMT 3B develops simultaneous DNA-methylation-related suppression and cytotoxic chemotherapy resistance for tumor suppressors and pro-apoptotic genes.[41] This test was conducted in compliance with the instructions using the EpiQuik DNA methyltransferase activity/inhibition test kit (Epigentek, Brooklyn, NY, USA). The ELISA assay kit was used to monitor two different concentrations of each test compound. Their enzyme inhibitory activity was measured using the colorimetric assay process. The experiment was carried out in duplicate for each concentration.[42]

Pharmacokinetic (ADME) Properties

The 2-D structures of compounds **4a**–**4j** were converted to 3D energy minimized structures using the Macro model module of Maestro 11.1. Qikprop module of Maestro11 was used to predict ADME properties. Some of the ADME properties that module predicts are but not limited to molecular weight, Lipinski rule of five, Lipinski rule of three, partition coefficient, aqueous solubility, oral bioavailability, dipole movement, SASA (total solvent accessible surface area), FOSA (hydrophobic component of the SASA), FISA (hydrophilic component of the SASA), skin permeability, CNS activity, blood-brain barrier permeability and blockage of HERG K+ channels.[43]

Molecular Dynamics Simulations

Molecular dynamic simulations were made using the DESMOND application provided by the D. E. Shaw group. All protein–ligand complexes were solvated in an orthorhombic box and were entrenched in the simple point charge (TIP3P) water model.[44] The system was neutralized with a counter ion such as Na^+ and Cl^- ion at a salt concentration of 0.15M. Subsequently, the system was relaxed using OPLS-2005 force field.[45,46] After several energy minimization steps, the equilibrated system was finally simulated for a period of 50 ns using isothermal–isobaric ensemble class to understand featured dynamics of small molecule during its interaction with selected molecule. The electrostatic interactions were determined during MD experiments using the Particle-Mesh-Ewald system.[47] The resultant MD trajectory was analyzed for stability of complex formation using different parameters such as RMSD, RMSF, SSE distribution of residual index, percentage of protein–ligand contacts and ligand torsion profile.

Supplementary Data

Further information relevant to the LC/MS and NMR spectra of compounds **4a**–**4j** is given in the *Supporting Information*. Crystallographic details for compound **4i** have been uploaded to the Cambridge Crystallographic Data Centre, CCDC No. 1949705. Copies of the

information can be accessed free of charge through a request to the CCDC, 12 Union Road, Cambridge CB2 1EZ, UK, e-mail: deposit@ccdc.cam.ac.uk.

Acknowledgements

DBT-NER BPMC, Sanctions Order No. BT/PR16268/NER/95/183/2015. The author acknowledges the financial support given for the venture. The authors thank Dr. K. Yeshoda Nanjappa for English correction and proof-reading. Arjun. H. A. is thankful to DBT for the Senior Research Fellow, and Dr. R. Elancheran is thankful for the support of DST-PURSE Phase II as Research Associate.

Author Contribution Statement

A.H.A., R.E., and S.K. conceived and designed the experiment. A.H.A. and N.M. performed the experiment. H.A., R.E., and K.L. analyzed the data. A.H.A. wrote the manuscript. M.R. and A.B. have done a critical revision of the manuscript for important intellectual content. R.E. carried out the analysis of single crystal XRD structures. R.K.R. performed the molecular dynamic simulations. All authors have contributed to the final version and approved the final manuscript.

References

[1] Facts & Figures, American Cancer Society, 2019, Atlanta, Ga.
[2] K. Dhananjaya, G. Sibi, H. Mallesha, K. R. Ravikumar, S. Awasthi, 'In silico studies of daidzein and genistein with human estrogen receptor α', *Asian Pac. J. Trop. Biomed.* **2012**, *2*, 1747–1753.
[3] K. Hermelink, 'Chemotherapy and Cognitive Function in Breast Cancer Patients: The So-Called Chemo Brain', *J. Natl. Cancer Inst. Monogr.* **2015**, *51*, 67–69.
[4] M. Morrow, H. J. Burstein, Harris, 'Malignant Tumors of the Breast', Principles and Practice of Oncology, 2015, Chapter 79, 10th edn.
[5] C. Dang, C. A. Hudis, 'Adjuvant Systemic Chemotherapy in Early Breast Cancer', Diseases of the Breast 2014, Chapter 44, 5th edn., Philadelphia: Wolters Kluwer Health.
[6] National Comprehensive Cancer Network (NCCN), Practice Guidelines in Oncology: Breast Cancer, 2017, Version 2, Accessed at www.nccn.org.
[7] A. C. Wolff, S. M. Domchek, N. E. Davidson, V. Sacchini, B. McCormick, 'Cancer of the Breast', Abeloff's Clinical Oncology, Elsevier 2014, Chapter 91, 5th edn.
[8] M. Motaghed, F. M. Al-Hassan, S. S. Hamid, 'Cellular responses with thymoquinone treatment in human breast cancer cell line MCF-7', *Phcog. Res.* **2013**, *5*, 200–206.
[9] V. L. Maruthanila, R. Elancheran, A. B. Kunnumakkara, S. Kabilan, J. Kotoky, 'Recent development of targeted approaches for the treatment of breast cancer', *Breast Cancer* **2017**, *24*, 191–219.
[10] H. Z. Zhang, L. L. Gan, H. Wang, C. H. Zhou, 'New progress in azole compounds as antimicrobial agents', *Mini-Rev. Med. Chem.* **2017**, *17*, 122–166.
[11] L. Zhang, X. M. Peng, G. L. V. Damu, R. X. Geng, C. H. Zhou, 'Comprehensive review in current developments of imidazole-based medicinal chemistry', *Med. Res. Rev.* **2014**, *34*, 340–437.
[12] L. L. Dai, S. F. Cui, G. L. V. Damu, C. H. Zhou, 'Recent advances in the synthesis and application of tetrazoles', *Chinese J. Org. Chem.* **2013**, *33*, 224–244.
[13] Y. Wang, C. H. Zhou, 'Recent advances in the researches of triazole compounds as medicinal drugs', *Sci. Sin. Chim.* **2011**, *41*, 1429–1456.
[14] C. H. Zhou, Y. Wang, 'Recent researches in triazole compounds as medicinal drugs', *Curr. Med. Chem.* **2012**, *19*, 239–280.
[15] H. Z. Zhang, J. J. Wei, K. V. Kumar, S. Rasheed, C. H. Zhou, 'Synthesis and biological evaluation of novel D-glucose-derived 1,2,3-triazoles as potential antibacterial and antifungal agents', *Med. Chem. Res.* **2014**, *24*, 182–196.
[16] J. C. P. Mayer, A. C. Sauer, B. A. Iglesias, T. V. Acunha, D. F. Back, 'Ferrocenylethenyl-substituted 1,3,4-oxadiazolyl, 1,2,4-oxadiazoles: synthesis, characterization and DNA-binding assays', *J. Organomet. Chem.* **2017**, *84*, 1–11.
[17] A. Sysak, B. O. Mrukowicz, 'Isoxazole ring as a useful scaffold in a search for new therapeutic agents', *Eur. J. Med. Chem.* **2017**, *137*, 292–309.
[18] G. Teresa, K. Szymankiewicz, P. Swiatek, 'Anti-Cancer Activity of Derivatives of 1,3,4-Oxadiazole', *Molecules* **2018**, *23*, 3361.
[19] H. Khalilullah, M. J. Ahsan, M. D. Hedaitullah, S. Khan, '1,3,4-Oxadiazole: A Biologically Active Scaffold', *Mini-Rev. Med. Chem.* **2012**, *12*, 789–801.
[20] B. Shalini, P. P. Roy, S. Singh, '1,3,4-Oxadiazoles as Telomerase Inhibitor: Potential Anticancer Agents', *Anti-Cancer Agents Med. Chem.* **2017**, *17*, 1869–1883.
[21] J. Mohamed, A. A. Choupraa, R. K. Sharmaa, S. S. Jadavb, 'Rationale Design, Synthesis, Cytotoxicity Evaluation, and Molecular Docking Studies of 1,3,4-oxadiazole Analogs', *Anti-Cancer Agents Med. Chem.* **2018**, *18*, 121–138.
[22] V. L. Maruthanila, R. Elancheran, N. K. Roy, A. Bhattacharya, 'In Silico Molecular Modelling of Selected Natural Ligands and Their Binding Features with Estrogen Receptor Alpha', *Curr. Comput.-Aided Drug Des.* **2019**, *15*, 89–96.
[23] Maestro, Schrödinger, 2016, LLC, New York, NY.
[24] F. Nique, S. Hebbe, C. Peixoto, D. Annoot, J. M. Lefrancois, 'Discovery of diarylhydantoins as new selective androgen receptor modulators', *J. Med. Chem.* **2012**, *55*, 8225–35.
[25] K. Lakshmithendral, K. Saravanan, R. Elancheran, K. Archana, N. Manikandan, H. A. Arjun, 'Design, synthesis and biological evaluation of 2-(phenoxymethyl)-5-phenyl-1,3,4-oxadiazole derivatives as anti-breast cancer agents', *Eur. J. Med. Chem.* **2019**, *168*, 1–10.

[26] G. M. Sheldrick, Shelx-97, 1997, Universitaet of Goettingen, Germany.
[27] G. M. Sheldrick, 'Crystal structure refinement with SHELXL', *Acta Crystallogr. Sect. C* **2015**, *71*, 3–8.
[28] G. M. Sheldrick, 'Phase Annealing in SHELX-90: Direct Methods for Larger Structures', *Acta Crystallogr. Sect. A* **1990**, *46*, 467.
[29] S. Divakar, K. Saravanan, P. Karthikeyan, R. Elancheran, S. Kabilan, 'Iminoenamine based novel androgen receptor antagonists exhibited anti-prostate cancer activity in androgen independent prostate cancer cells through inhibition of AKT pathway', *Chem.-Biol. Interact.* **2017**, *275*, 22–34.
[30] B. Plouvier, R. Houssin, N. Helbecque, P. Colson, C. Houssier, 'Influence of the methyl substituents of a thiazole-containing lexitropsin on the mode of binding to DNA', *Anti-Cancer Drugs* **1995**, *10*, 155–166.
[31] S. B. Baylin, 'DNA methylation and gene silencing in cancer', *Nat. Rev. Clin. Oncol.* **2005**, *2*, 4–11.
[32] Schrödinger, QikProp 2019–3, LLC, New York, NY.
[33] S. A. A. Anand, C. Loganathan, K. Saravanan, S. Kabilan, 'Comparison of Molecular Docking and Molecular Dynamics Simulations of 1,3-Thiazin-4-one with MDM2 Protein', *Int. Lett. Chem. Phys. Astron.* **2015**, *60*, 161–167.
[34] Schrödinger, Maestro, 2016 LLC, New York, NY.
[35] R. Chen, 'MTT Assay of Cell Numbers after Drug/Toxin Treatment', *Bio-101* **2011**, e51.
[36] T. Hayon, A. Dvilansky, O. Shpilberg, I. Nathan, 'Appraisal of the MTT-based assay as a useful tool for predicting drug chemo sensitivity in leukemia', *Leuk. Lymphoma* **2003**, *44*, 1957–1962.
[37] T. Afsar, J. H. Trembley, C. E. Salomon, S. Razak, M. R. Khan, K. Ahmed, 'Growth inhibition and apoptosis in cancer cells induced by polyphenolic compounds of *Acacia hydaspica*: Involvement of multiple signal transduction pathways', *Sci. Rep.* **2016**, *6*, 1–12.
[38] S. Maliheh, N. Esmati, S. K. Ardestani, S. Emami, S. Ajdari, 'Halogenated flavones as potential apoptosis-inducing agents: synthesis and biological activity evaluation', *Eur. J. Med. Chem.* **2012**, *58*, 573–580.
[39] M. Sameer, 'Expression of DNA Methyltransferases in Breast Cancer Patients and to Analyze the Effect of Natural Compounds on DNA Methyltransferases and Associated Proteins', *J. Breast Canc.* **2013**, *16*, 23–31.
[40] D. Raluca, 'Roles of glutathione-S-transferase P1 (GSTP1) gene, in prostate cancer detection', *J. Pediatr.* **2009**, *12*, 47–48.
[41] S. Rupninder, 'Dysregulation of the Epigenome in Human Breast Cancer', *Am. J. Pathol.* **2015**, *185*, 282–292.
[42] K. D. Robertson, 'DNA methylation and chromatin: unraveling the tangled web', *Oncogene* **2002**, *21*, 5361–5379.
[43] H. A. Arjun, R. Elancheran, N. Manikandan, K. Lakshmithendral, M. Ramanathan, 'Design, Synthesis, and Biological Evaluation of (*E*)-*N*'-((1-Chloro-3,4-dihydronaphthalen-2-yl) methylene)benzohydrazide Derivatives as Anti-prostate Cancer Agents', *Front. Chem.* **2019**, *7*, 474.
[44] W. L. Jorgensen, J. Chandrasekhar, J. D. Madura, R. W. Impey, M. L. Klein, 'Comparison of simple potential functions for simulating liquid water', *J. Chem. Phys.* **1983**, *79*, 926–935.
[45] W. G. Hoover, 'Canonical dynamics: Equilibrium phase-space distributions', *Phys. Rev. A* **1985**, *31*, 1695–1697.
[46] G. J. Martyna, D. J. Tobias, M. L. Klein, 'Constant pressure molecular dynamics algorithms', *J. Chem. Phys.* **1994**, *101*, 4177–4189.
[47] U. Essmann, L. Perera, M. L. Berkowitz, T. Darden, H. Lee, L. G. Pedersen, 'A smooth particle mesh Ewald method', *J. Chem. Phys.* **1995**, *103*, 8577–8859.

Received November 20, 2019
Accepted January 7, 2020

